RSC Advances

PAPER

View Article Online
View Journal | View Issue

Cite this: *RSC Adv.*, 2025, **15**, 29989

In situ encapsulation of coumarin/fluorescent bleacher/carbazole derivatives@Eu MOF materials for white light-emitting diodes

Xin-Yu Liu,[a] Shu-Jing Zhou(Co-author),[ab] Fang Luan,[ab] Yu-Hang Wang,[ab] Xiu-Juan Ma,[a] Li-Yuan Sui[ab] and Yan-Ru Feng *[ab]

Metal-organic frameworks (MOFs), characterized by their high porosity, large specific surface area, and tunable pore structures, have emerged as promising host materials for advanced functional applications. In this study, two organic dyes, fluorescent bleacher (CBS) and coumarin (C6), exhibiting blue and green fluorescence, respectively, were co-encapsulated into europium (Eu)-based MOFs, where Eu^{3+} served as the central metal to introduce red emission. The ligand employed was 9-butylcarbazole-2-carboxylhydrazide thiophene (Cz). A white fluorescent powder, coumarin/fluorescent bleacher/carbazole derivatives@Eu (C6/CBS/Cz@Eu), was synthesized using an *in situ* encapsulation method. The C6/CBS/Cz@Eu was incorporated into PVA to prepare a film. The resulting C6/CBS/Cz@Eu film demonstrated a high-quality white light emission under excitation by commercial 400 nm light-emitting diode (LED) chips, achieving ideal Commission Internationale de l'Éclairage (CIE) chromaticity coordinates of (0.34, 0.35) and a correlated color temperature (CCT) of 5267 K. This strategy offers a versatile and scalable method for the design and fabrication of white light-emitting materials, beneficial for the development of next-generation white light-emitting diode (WLED) technologies.

Received 31st May 2025
Accepted 1st August 2025

DOI: 10.1039/d5ra03849a

rsc.li/rsc-advances

1 Introduction

In recent decades, the growing demand for efficient and environmentally sustainable light sources has positioned solid-state lighting (SSL) as a critical component of modern life. Among various SSL technologies, white light-emitting diodes (WLEDs) have emerged as the most promising candidates due to their high luminous efficiency,[1] extended operational lifespan,[2] low power consumption,[3] and minimal environmental impact.[4] These advantages enable WLEDs to play a pivotal role in both general lighting and display technologies.[5] Commercial WLEDs are typically fabricated by combining a blue LED chip with a yellow-emitting phosphor. However, this conventional approach suffers from significant drawbacks, including poor color temperature stability and suboptimal luminous efficiency.[6]

To improve the white-light performance of WLEDs, numerous strategies have been explored to incorporate fluorescent powders into diverse host matrices. Among these, metal-organic frameworks (MOFs) have garnered significant attention. MOFs are a class of nanoporous crystalline materials that are constructed from metal ions or clusters coordinated with organic ligands.[7] The concept of MOFs gained widespread recognition in the mid-1990s when Tranchemontagne, D *et al.*[8] synthesized layered compounds exhibiting reversible gas adsorption properties. Kitagawa, S *et al.*[9] introduced three-dimensional MOFs capable of reversible gas uptake at room temperature. Due to their tunable luminescence, high thermal and chemical stability, and structural versatility, MOFs have emerged as excellent fluorescent materials for various photonic applications.[10] Their well-defined pore architecture and modular composition make them particularly attractive as host matrices for dye encapsulation in advanced luminescent systems.

Ligands employed in the construction of MOFs include carboxylate compound salts[11] and heterocyclic compounds.[12] Among these, carbazole (Cz) and its derivatives represent a versatile class of nitrogen (N)-containing aromatic compounds with a wide range of applications, including photocatalysis,[13] organic dye synthesis,[14] agrochemical development,[15] and supramolecular recognition.[16] Structurally, Cz features a rigid π-conjugated system, where the N atom acts as a key coordination site,[17] enabling interactions with metal ions or guest molecules. Furthermore, the Cz framework allows for facile functionalization with a variety of electron-donating or electron-withdrawing groups, such as hydrazine, thiophene, and pyridine. These modifications offer a means to fine-tune the electronic configuration and photophysical behavior of the resulting materials. Therefore, Cz-based ligands exhibit excellent thermal stability and optoelectronic performance, making

[a]*College of Pharmacy, Jiamusi University, Jiamusi 154007, China*
[b]*Heilongjiang Provincial Key Laboratory of New Drug Development and Pharmacotoxicological Evaluation, Jiamusi 154007, China*

them ideal candidates for the development of next-generation luminescent and nonlinear optical materials.

Wang *et al.*[18] synthesized N-doped carbon dots (N-CDs) through a solvothermal method and integrated them with aluminum-based frameworks using an *in situ* hydrothermal method to fabricate a composite material denoted as MIL-53(Al)-NH_2@N-CDs. With the unique fluorescence characteristics of this hybrid structure, the researchers developed an LED device exhibiting adjustable multicolor emission, presenting a promising strategy for the advancement of high-performance, tunable LED technologies. Wei *et al.*[19] prepared three types of dye-loaded MOF composites through an encapsulation technique. In particular, they embedded eosin Y (EY), a fluorescent dye, into zirconium (Zr)-based MOFs (DUT-52), yielding a self-calibrating fluorescence sensor for pesticide detection. This study highlighted a new and effective platform for applications in chemical sensing and environmental monitoring. Hu *et al.*[20] designed and synthesized a series of rare earth metal-organic frameworks based on carbazole. White light emission was achieved by adjusting the molar ratios of Eu^{3+}, Tb^{3+}, and Y^{3+}. It can be used as a temperature sensor, exhibiting excellent luminescence and color-change sensing capabilities for dimethylformamide (DMF). Liu *et al.*[21] prepared a dual-luminescent composite material comprising europium-based metal-organic frameworks and coumarin 7 using solvothermal method and post-modification strategy. They researched their reusability and temperature sensing mechanism, indicating the potential of Eu-MOF complexes functionalized with coumarin 7 as dual-mode optical thermometers for temperature sensing applications.

Despite these developments, the most commonly employed approach for dye loading in MOFs remains the immersion method. This technique, which typically relies on electrostatic adsorption, is susceptible to environmental fluctuations that can compromise reproducibility and material stability. Furthermore, the electrostatically adsorbed dyes often necessitate post-synthesis curing to ensure structural integrity. In contrast, the *in situ* encapsulation technique (also referred to as the "one-pot method") incorporates all essential components (*e.g.*, metal ions, ligands, and guest molecules) during the MOF synthesis. This strategy facilitates the direct formation of coordination bonds between the guest dye and the metal centers, yielding structurally robust composites with superior optical and thermal stability.

Most MOF crystals are typically obtained in their powder form, which poses obvious limitations for their direct application in optical sensors and optoelectronic devices. Specifically, when integrated with WLED chips, the powdered composite materials require additional processing steps such as mixing, dispersion, and coating, which can introduce complexity and variability into the fabrication process.[20] To overcome these challenges and broaden the practical applicability of MOF-based luminescent systems, it is necessary to develop its films capable of delivering stable and high-quality white light emission.

In this study, europium (Eu^{3+}) was selected as the central metal ion, and 9-butylcarbazole-2-carboxylic acid thiophene served as the organic ligand for constructing MOF materials using a solvothermal synthesis method. The resulting MOFs were further functionalized through an *in situ* encapsulation strategy to incorporate coumarin (C6) and CBS dyes, yielding a composite luminescent material. By tuning the feed ratio of the incorporated dyes, the emission characteristics of the resulting MOF-based system can be modulated to achieve high-quality white light emission. This approach offers a pathway for the development of luminescent materials for use in SSL applications.

2 Experimental

2.1. Chemicals and materials

Europium nitrate hexahydrate ($Eu(NO_3)_3 \cdot 6H_2O$) was obtained from Shanghai Macklin Biochemical Co., Ltd The organic dyes C6 and CBS, along with polyvinyl alcohol (PVA), were purchased from Aladdin Reagents. Absolute ethanol was supplied by Sinopharm Chemical Reagent Co., Ltd All reagents were of analytical grade and were used as received, without further purification.

2.2. Instruments and measurements

The morphology and particle size distribution of the synthesized samples were examined using scanning electron microscopy (SEM, Hitachi Regulus 8100, Japan) and transmission electron microscopy (TEM). The elemental composition and spatial distribution of Cz@Eu and C6/CBS/Cz@Eu microstructures were analyzed by energy-dispersive X-ray spectroscopy (EDS, EDAX Octane Elect Super, 70 mm, USA). X-ray photoelectron spectroscopy (XPS, ESCALAB 250Xi, Thermo Fisher Scientific, USA) was employed to characterize the chemical composition and bonding states of the samples. Crystalline structures were analyzed using powder X-ray diffraction (XRD) using an X'Pert PRO diffractometer (Shimadzu XRD-6000) with Cu-Kα radiation over a 2θ range of 5°–50°. Thermogravimetric analysis (TGA) was performed under a N_2 atmosphere to assess the thermal stability, indicating that C6/CBS/Cz@Eu remains stable up to ~500 °C. Fourier-transform infrared spectroscopy (FTIR, Spectrum Two, PerkinElmer, USA) was used to identify functional groups and verify chemical structures. Fluorescence spectra were recorded using a fluorescence spectrophotometer (F-7100, Hitachi High-Technologies, Japan).

2.3. Synthesis of Cz@Eu

To synthesize Cz@Eu, 0.3059 g of $Eu(NO_3)_3 \cdot 6H_2O$ and 0.1003 g of 9-butylcarbazole-2-carboxylic acid thioether were dissolved in 30 mL of anhydrous ethanol in a polytetrafluoroethylene (PTFE)-lined stainless steel autoclave (KH-100, China). The sealed reactor was heated at 150 °C for 24 h, then allowed to cool naturally to room temperature. The resulting yellowish suspension was centrifuged at 8000 rpm for 30 min (TG-18, Sichuan, China), and the precipitate was washed with ethanol and ultrapure water to remove any unreacted precursors. The purified product was then dried under vacuum at 60 °C for 10 h, yielding a yellowish powder (C, 8.755; H, 1.753; N, 1.435; S, 0.716%).

2.4. Synthesis of C6/CBS/Cz@Eu

The synthesis procedures for C6/Cz@Eu and CBS/Cz@Eu are detailed in the SI. For the preparation of the ternary composite C6/CBS/Cz@Eu (Fig. 1a), 0.3059 g of $Eu(NO_3)_3 \cdot 6H_2O$, 0.1003 g of 9-butylcarbazole-2-carboxylic acid thiophene, 0.001 g of C6, and 0.003 g of CBS were dissolved in 60 mL of anhydrous ethanol within a PTFE-lined stainless steel autoclave (KH-100, Sichuan, China). The sealed reactor was heated at 150 °C for 24 h and then allowed to cool to room temperature. The resulting product was centrifuged at 8000 rpm (TG-18, Sichuan, China) for 30 min. The collected precipitate was washed with ethanol and ultrapure water, then dried under vacuum at 60 °C for 10 h to obtain a dark yellow crystalline solid (C, 19.58; H, 2.527; N, 1.41; S, 0.713%)

2.5. Synthesis of luminescent films C6/CBS/Cz@Eu (Mw. 85 000–124 000)

To fabricate the luminescent film, 1.0 g of PVA (Mw. 85 000–124 000) was dissolved in 50 mL of distilled water in a round-bottom flask. Subsequently, 100 mg of C6/CBS/Cz@Eu powder was added to the solution. The mixture was maintained at 85 °C in an oil bath and stirred continuously for 2 h to ensure uniform dispersion. The resulting injection molding fluid was then cast onto a quartz plate and vacuum-dried at 60 °C for 3 h to form a solid C6/CBS/Cz@Eu film.

2.6. White glowing demonstration

The optimized C6/CBS/Cz@Eu thin film, cast onto a quartz substrate, was mounted on a commercial near-ultraviolet (UV, 400-nm) LED chip.

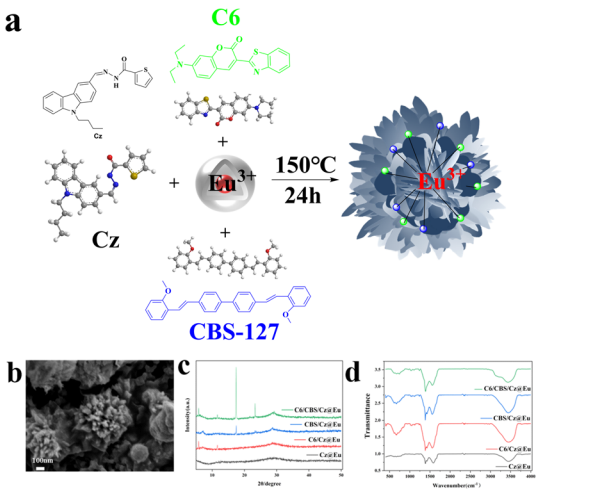

Fig. 1 (a) Simulated composite structure diagram of C6/CBS/Eu@Cz. (b) SEM image of C6/CBS/Cz@Eu. (c) XRD patterns and (d) Fourier transform infrared spectra of Eu@Cz, C6/Eu@Cz, CBS/Eu@Cz, and C6/CBS/Eu@Cz.

3 Results and discussion

3.1. Physical characterization

The morphology of the synthesized materials was investigated using SEM and TEM. As shown in Fig. S1a, Cz@Eu formed uniformly spherical particles with an average diameter of ~200 nm. In contrast, SEM image of C6/Cz@Eu (Fig. S1b) revealed smooth, spherical MOF structures with an increased particle size of ~400 nm, suggesting successful incorporation of the C6 dye. Similarly, CBS/Cz@Eu (Fig. S1c) exhibits rough-surfaced spherical particles, also ~400 nm in size. Remarkably, co-encapsulation of both dyes in the C6/CBS/Cz@Eu composite (Fig. 1b) produced a different nanoflower-like morphology while preserving the ~400 nm dimension. This hierarchical structure not only contributes to improved structural stability but also enhances the specific surface area by offering more accessible active sites. TEM images (Fig. S1d and e) further confirmed the uniform spherical structure of Cz@Eu and the distinct morphological features of the C6/CBS/Cz@Eu composite. Preliminary results from SEM and TEM confirm the successful synthesis of C6/CBS/Cz@Eu.

Comparative EDS and elemental mapping analyses of Cz@Eu (Fig. S2–S4) confirm the presence of C, N, O, Eu, and S. Similarly, the elemental mapping of C6/CBS/Cz@Eu (Fig. 3) indicates the presence of these elements.

Combining FTIR results (Fig. 1d) for the ternary composite C6/CBS/Cz@Eu, a characteristic hydrazide N–H stretching vibration is observed at ~3500 cm^{-1}, along with a metal–oxygen (Eu–O) stretching band in the 500–600 cm^{-1} range, and the C=O stretching vibration confirms the successful coordination between Eu^{3+} and the organic ligand. XRD analysis was conducted using a MiniFlex 2 diffractometer with Cu-Kα radiation ($\lambda = 0.1542$ nm) at a scanning rate of 10° min^{-1} over a 2θ range of 3°–50°. The resulting diffraction patterns for Cz@Eu, C6/Cz@Eu, CBS/Cz@Eu, and C6/CBS/Cz@Eu are depicted in Fig. 1c. In Fig. S5, the XRD pattern of Cz@Eu shows diffraction peaks corresponding to Cz; the XRD pattern of C6/Cz@Eu shows a C6 diffraction peak; and the XRD pattern of CBS/Cz@Eu shows diffraction peaks corresponding to CBS. These results indicate that Cz@Eu, C6/Cz@Eu and CBS/Cz@Eu were successfully prepared. The XRD pattern of C6/CBS/Cz@Eu closely aligns with those of both C6/Cz@Eu and CBS/Cz@Eu, indicating that the crystallinity of the framework is retained following dye encapsulation. The consistency of these diffraction peaks confirms the successful formation of the ternary composite material. These results provide preliminary confirmation of the successful synthesis and co-encapsulation of C6/CBS/Cz@Eu.

The XPS spectrum of the C6/CBS/Cz@Eu composite (Fig. 2) confirms the presence of C, N, O, Eu, and S. Compared with Cz@Eu high-resolution XPS spectra (Fig. S6), the Eu $3d_{5/2}$, N 1s, and O 1s peaks remain consistent with those observed in Cz@Eu, suggesting preservation of the coordination environment. However, two additional peaks appear in the C 1s region at 285.74 eV and 295.53 eV, corresponding to C–S and C=O–S bonds, respectively. These features provide strong evidence for

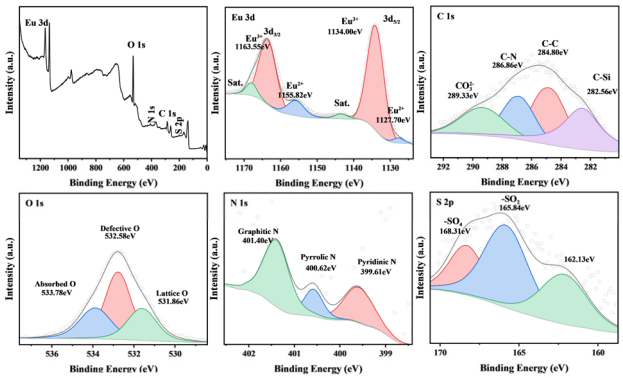

Fig. 2 XPS full spectrum and high resolution XPS spectra of Eu 3d, C 1s, O 1s, N 1s, and S 2p of C6/CBS/Cz@Eu.

successful incorporation of S-containing groups from the C6 dye into the MOFs framework.

3.2. Stability properties of materials

3.2.1. Thermal stability properties of materials. Thermal stability was evaluated using TGA, which measures the mass loss of a material as a function of temperature, providing insights into structural decomposition and thermal events (*e.g.*, endothermic or exothermic transitions). TGA confirms that the C6/CBS/Cz@Eu composite exhibits excellent thermal stability. TGA was performed on Cz@Eu, C6/Cz@Eu, CBS/Cz@Eu and C6/CBS/Cz@Eu, and the resulting curves are presented in Fig. S7. For the four samples, an initial weight loss is observed at ~100 °C, corresponding to the desorption of physically adsorbed water molecules. A second significant weight loss occurs between 200 °C and 400 °C, which is attributed to the removal of residual solvent (anhydrous ethanol) within the MOF pores and the decomposition of organic linkers. Notably, the decomposition of the MOF framework in Cz@Eu, C6/Cz@Eu and CBS/Cz@Eu occurs slightly earlier than in the C6/CBS/Cz@Eu composite, indicating a marginal improvement in thermal stability upon dye encapsulation. A third major weight loss is observed above 400 °C, signifying the complete breakdown of the MOF structure. Overall, the thermal decomposition profiles of Cz@Eu and C6/CBS/Cz@Eu are highly comparable; C6/CBS/Cz@Eu remains relatively stable within a certain temperature range and demonstrates relatively good thermal stability. Significant mass loss only begins to occur at higher temperatures, indicating that its structure is less likely to be damaged in a hot environment, suggesting that the incorporation of C6 and CBS dyes does not compromise the structural integrity or thermal robustness of the composite material.

3.2.2. Chemical stability of materials. Figure S8 shows the chemical stability of C6/CBS/Cz@Eu prepared by *in situ* encapsulation and impregnation methods in organic solvents, assessed by UV spectrophotometry. For both preparation methods, the same mass of material was dispersed in the same volume of anhydrous ethanol and subjected to three ultrasonic treatments at 1-h intervals. The resulting suspension was filtered, and the UV absorption spectra were recorded. The *a* and *b* absorption curves correspond to the UV absorption spectra of samples *c* and *d*, respectively. The absorption curve of a showed absorption peaks at 360 nm and 455 nm, and literature review revealed that they were the UV characteristic absorption peaks of CBS and C6, respectively. This indicates that the material prepared by the impregnation method had already dissolved most of the dyes into the solution. The absorption curve *b* also showed a weak UV characteristic absorption peak of CBS at 360 nm, suggesting that CBS material is not suitable as a ligand and that a fraction of CBS dyes has decomposed. These results indicate that the *in situ* encapsulation method used in this study provides better chemical stability than the material prepared by impregnation method. C6/CBS/Cz@Eu also showed good stability.

3.3. Fluorescence properties of Eu-MOFs

3.3.1. Cz and Cz@Eu fluorescence properties. Fig. S9a illustrates the fluorescence spectra of the ligand 9-butylcarbazole-2-carboxylic acid hydrazide thiophene and the Cz@Eu complex. Under excitation at 350 nm, the ligand Cz exhibits a broad emission band centered at ~460 nm, corresponding to a blue fluorescence. Upon coordination with Eu^{3+} to form Cz@Eu, the emission shows four peaks at 428 nm, 450 nm, 535 nm, and 620 nm. This spectral broadening and red-shift indicate a significant enhancement in luminescent properties resulting from metal–ligand interactions within the MOF structure. The colorimetric behavior of the materials was further analyzed using the Commission Internationale de l'Éclairage (CIE) 1931 chromaticity diagram. The CIE (*x*, *y*) coordinates of the Cz ligand shift from (0.45, 0.26) to (0.48, 0.44) in Cz@Eu (Fig. 3a and b), reflecting a clear transition from blue to red emission. These results confirm the successful coordination of the Cz-based ligand with Eu^{3+} and demonstrate the potential of Cz@Eu as a tunable fluorescent material for photonic applications.

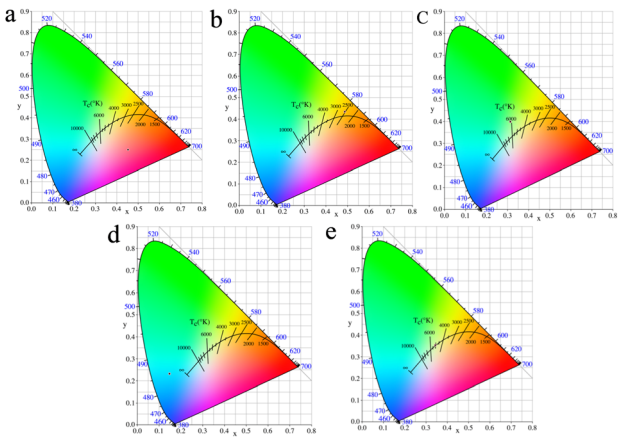

Fig. 3 (a) Color temperature image of Cz. (b) Color temperature image of Cz@Eu. (c) Color temperature image of C6/Cz@Eu. (d) Color temperature image of CBS/Cz@Eu. (e) Color temperature image of C6/CBS/Cz@Eu.

3.3.2. C6 and C6/Cz@Eu fluorescence properties. C6 is a widely studied and highly efficient organic fluorescent dye known for its strong green emission, making it a promising candidate for use as a green light-emitting unit. In Fig. S8b, C6 shows a broad emission band centered at ~575 nm when excited at 300 nm. Under 300 nm excitation, the pristine C6/Cz@Eu exhibits characteristic peaks at 490 nm, 545 nm, and 615 nm, associated with Eu-based transitions. However, upon C6 encapsulation, the emission spectrum of the composite shifts from the original red-dominated profile to one exhibiting a pronounced green luminescence. The CIE 1931 (x, y) chromaticity coordinates of C6/Cz@Eu are (0.31, 0.39) (Fig. 3c), consistent with a strong green emission. These results confirm the successful incorporation of C6 into the MOF matrix and demonstrate its capability to modulate the photoluminescent properties of the host material. Therefore, C6 serves as an effective green luminescent unit for developing MOF-based materials aimed at high-quality white light emission.

3.3.3. CBS and CBS/Cz@Eu fluorescence properties. Further investigations were conducted to evaluate the integration of blue-emitting guest molecules into the Cz@Eu framework, a critical step toward achieving full-spectrum white light emission. Fluorescent brighteners such as CBS-127 are known for their strong blue luminescence in both solid and solution phases. In this study, CBS was selected as a representative blue-emitting dye. In Fig. S9c, CBS exhibits broad emission bands centered at 360 nm and 385 nm under 350 nm excitation. When embedded within the Cz@Eu framework and excited at 450 nm, the CBS/Cz@Eu composite shows three emission peaks at 425 nm, 460 nm, and 485 nm, indicating a significant shift in the emission profile from the red-dominated spectrum of Cz@Eu to the blue region. The chromaticity coordinates of CBS/Cz@Eu, as determined from the CIE 1931 diagram (Fig. 3d), are (0.25, 0.35), confirming its blue luminescent characteristics. These results validate the effective encapsulation of CBS into the MOF structure and highlight its potential as a blue light-emitting component.

3.3.4. C6/CBS/Cz@Eu fluorescence properties. C6/Cz@Eu and CBS/Cz@Eu have been previously demonstrated as effective green- and blue-emitting systems, respectively. To achieve white light emission, both dyes were co-encapsulated within the Cz@Eu framework using a one-pot *in situ* synthesis approach, resulting in the successful formation of the ternary composite C6/CBS/Cz@Eu. In Fig. S9d, the emission spectrum of C6/CBS/Cz@Eu under 400 nm excitation spans nearly the entire visible range, combining blue, green, and red emissions. This broad-spectrum luminescence results in a composite material with CIE 1931 chromaticity coordinates of (0.34, 0.35) and a moderate correlated color temperature (CCT) of 5267 K in Fig. 3e, closely approximating the ideal white light coordinates of (0.33, 0.33). The high CCT (5000 K–6500 K) of LEDs corresponds to cool white, close to natural light, with clearer and sharper light, suitable for environments such as offices and study rooms that require focus and efficient work, and can also reduce visual fatigue. The spectral balance and stability achieved through co-encapsulation validate the synergistic interaction of the dyes within the MOF matrix. These results underscore the potential of C6/CBS/Cz@Eu as a high-performance white fluorescent powder.

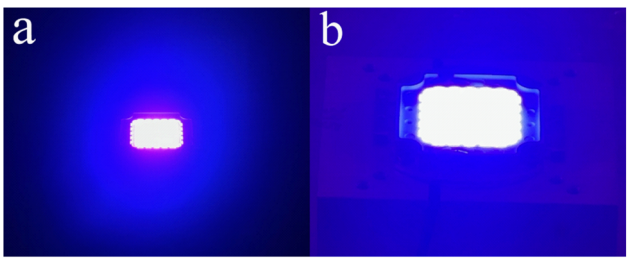

Fig. 4 (a) Photograph when a 400 nm LED chip is turned on (b) by C6/CBS/Cz@Eu. (b) Photograph of a rough white light-emitting LED assembled with a thin film of C6/CBS/Cz@Eu on a 400-nm LED chip.

3.4. Manufacturing of coarse WLED

In Fig. S10,we used the same slit width and gain, with 400 nm as the excitation wavelength, and separately detected the fluorescence properties of Cz@Eu, C6/Cz@Eu, CBS/Cz@Eu and C6/CBS/Cz@Eu. We calculated the CIE color temperature values of four materials based on their fluorescence properties (Fig. S11). Fig. 4a illustrates an operational image of a 400-nm LED chip, while Fig. 4b depicts the assembled WLED incorporating a thin-film composite of C6/CBS/Cz@Eu. The luminescent film was fabricated by dispersing the C6/CBS/Cz@Eu composite within a PVA matrix. This film exhibited high-quality white emission, along with excellent thermal stability and sustained luminescent performance under continuous operation. For practical device implementation, the composite film was directly applied onto a 30 W ultraviolet-visible (UV-vis) LED chip array (400 nm excitation). Upon activation, the device emitted bright white light with CIE 1931 chromaticity coordinates of (0.34, 0.35), closely approximating the ideal white point of (0.33, 0.33). These results demonstrate the efficacy of the C6/CBS/Cz@Eu composite as a robust and efficient white-light-emitting material, affirming its promise for integration into next-generation SSL technologies.

4 Conclusions

In summary, C6 and CBS dyes were co-encapsulated into self-synthesized Eu-based MOFs (Cz@Eu) through an *in situ* encapsulation method. This method effectively addressed the common challenge of poor stability in dye-loaded MOF materials and enabled the development of high-quality WLEDs. Upon excitation at 400 nm, the C6/CBS/Cz@Eu composite exhibited bright, well-balanced white light emission. By embedding the composite into a PVA matrix and applying it to a 400-nm LED chip, a functional WLED device was fabricated. The device achieved optimal CIE coordinates of (0.34, 0.35) and a moderate correlated color temperature (CCT) of 5267 K, confirming its suitability for practical lighting applications. Importantly, this facile and versatile synthetic strategy allows for the incorporation of other luminescent guest molecules,

offering extensive tunability in both structural and photophysical properties. Given the vast diversity of porous MOF architectures and fluorescent dyes, this method provides a scalable pathway for designing novel white-light-emitting composites. The realization of stable, high-performance white light emission in this work makes a little progress in advancing next-generation SSL technologies.

Author contributions

Xin-Yu Liu: writing – original draft. Shu-Jing Zhou, formal analysis, conceptualization, writing – original draft. Fang Luan: validation, data curation. Yu-Hang Wang: resources, review and validation. Xiu-Juan Ma: editing and validation, formal analysis. LiYuan Sui: editing and validation, formal analysis. Yan-Ru Feng: writing – review & editing, funding acquisition, supervision, project administration.

Conflicts of interest

The authors declare that they have no known competing financial interests or personal relationships that could have appeared to influence the work reported in this paper.

Data availability

The data will be made available upon reasonable request.

The SI provides the synthesis methods, characterizations (including SEM, TEM, EDS, XRD, and XPS), and stability tests of materials. See DOI: **https://doi.org/10.1039/d5ra03849a**.

Acknowledgements

This research was supported by the Heilongjiang Provincial Education Department Basic Scientific Research Funds (2019-KYYWF-1343), Jiamusi University Doctoral Research Start-up Foundation (JMSUBZ2019-12), and Open project of Heilongjiang Provincial Key Laboratory of New Drug Development and Pharmacotoxicological Evaluation (kfkt2022-04). The authors would like to express their gratitude for the assistance and financial support received from Jiamusi University.

References

1 (*a*) Y. You, Y. Zheng and Z. Pan, *J. Lumin.*, 2025, **277**, 120984; (*b*) J. W. Jing, L. F. Zhe and S. Guangyi, *Nat. Photonics*, 2023, **18**, 200.
2 (*a*) J. Shi, Y. Chen and G. Miao, *Mater. Sci. Semicond. Process.*, 2025, **186**, 109090; (*b*) M. Turhal, C. Albayrak and Y. Mahmutoglu, *Phys. Comm.*, 2024, **67**, 102511.
3 (*a*) Z. Y. He, S. C. Ma and H. Yin, *Commun. Phys.*, 2024, **7**, 362; (*b*) Z. Abdelhakim, B. Abdelber and S. Helima, *Optik*, 2022, **190**, 269.
4 (*a*) X. Guan, Y. Li and Y. Meng, *Nat. Commun.*, 2024, **15**, 9913; (*b*) J. Huang and R. Nie, *Heliyon*, 2024, **10**, e33020.
5 (*a*) A. Zhang, Y. Zhu and Z. Sun, *Semicond. Technol.*, 2024, **49**, 953; (*b*) J. Kai, N. Lunshuai and G. Yixi, *Inorg. Chem. Commun.*, 2024, **160**, 111858.
6 (*a*) H. Hou, C. Liu and F. Liu, *Chin. J. Laser*, 2023, **50**, 75; (*b*) Y. V. Kuznetsova and I. D. Popov, *Ceram. Int.*, 2022, **48**, 18972.
7 (*a*) M. Sun, Yu Ruili and H. Sun, *Isotopes*, 2024, 488; (*b*) L. Zhang, Y. Feng and C. Weng, *Inorg. Chem.*, 2024, **63**, 17357.
8 D. Tranchemontagne, J. L. Mendoza-Cortes, M. O'Keefe and O. M. Yaghi, *Chem. Soc. Rev.*, 2009, **38**, 1257.
9 S. Kitagawa, R. Kitaura and S. Noro, *Angew. Chem., Int. Ed.*, 2004, **43**, 2334.
10 (*a*) Q. Yuxuan, Z. Chenglong and C. Zhiquan, *Inorg. Chem.*, 2023, **62**, 8315; (*b*) C. Mengyun, S. Rong and W. Qiongqiong, *Polyhedron*, 2023, **235**, 116; (*c*) C. Jie, J. Xin and F. Yangchun, *Materials*, 2022, **15**, 7933.
11 (*a*) F. Keshavarz, E. Mazarei and A. Noubir, *Comput. Mater. Sci.*, 2025, **247**, 113551; (*b*) S. O. Bull, *Eur. J. Chem.*, 2024, **15**, 71.
12 (*a*) D. Ma, N. Li and D. Zhu, *J. Hazard. Mater.*, 2024, **480**, 136148; (*b*) S. Joshi, S. Asthana and D. M. Pandey, *J. Mol. Struct.*, 2025, **1319**, 139469.
13 (*a*) K. Verma, M. A. Addicoat and K. R. Justin Thomas, *ACS Appl. Polym. Mater.*, 2024, 3909; (*b*) A. F. Saber, A. M. Elewa and H. H. Chou, *Appl. Catal., B*, 2022, **316**, 121624; (*c*) G. Wei, L. Wang and Z. Ding, *J. Colloid Interface Sci.*, 2023, **642**, 648.
14 (*a*) D. Devadiga, M. Selvakumar and P. Shetty, *Int. J. Energy Res.*, 2021, **45**, 6584; (*b*) R. Munir, A. F. Zahoor and M. N. Anjum, *Top. Curr. Chem.*, 2025, **383**, 5.
15 (*a*) W. Pan, G. G. Chen and Z. Y. Zhang, *Spectrochim. Acta, Part A*, 2022, **268**, 120644; (*b*) S. A. Patil, S. A. Patil and E. A. Ble-González, *Molecules*, 2022, **27**, 6575.
16 (*a*) Y. Zhai, Y. Wang and X. Zhu, *Macromolecules*, 2021, **54**, 5249; (*b*) O. S. Tiwari, V. Rawat and S. Rencus-Lazar, *Spectrochim. Acta, Part A*, 2025, **326**, 125277.
17 X. Liu, J. Shang and J. Li, *Angew. Chem.*, 2025, **137**, e202420160.
18 H. Wang, Li Huijun and Li Ying, *Nonferrous Met. Mater. Eng.*, 2024, **190**, 1.
19 Z. Wei, D. Chen and Z. Guo, *Chem*, 2020, **59**, 5386.
20 Y. Hu, R. S. H. Khoo and J. Lu, *ACS Appl. Mater. Interfaces*, 2022, **14**, 41178–41185.
21 J. Liu, X. Yue and Z. Wang, *J. Mater. Chem. C*, 2020, **8**, 13328–13335.